

Hydrodynamic-model calculation of second-harmonic generation at a metal surface

M. Corvi and W. L. Schaich

Physics Department and Materials Research Institute, Indiana University, Bloomington, Indiana 47405

(Received 21 October 1985)

Using a hydrodynamic model of collective electronic motion we calculate the efficiency of second-harmonic generation in a simple reflection geometry. The model applies to a smooth, jellium metal surface, which is treated as having a sequence of steps in the equilibrium electron-density profile. We derive both the equations of motion and additional boundary conditions necessary for our approach. The final formulas are numerically evaluated for various values of the system's parameters. The results show considerable variation with frequency, especially when multipole modes are present in the linear response. We demonstrate that the general results can be usefully parametrized in terms of bulk optical properties and a pair of complex, frequency-dependent parameters that summarize the response at the surface.

I. INTRODUCTION

In recent years considerable theoretical work has been devoted to the linear electrodynamic response of a jellium surface.¹⁻⁶ One has developed a good qualitative understanding of the local-field effects due to the vacuum-metal interface, and detailed calculations have been performed. Our effort in this paper is directed towards extending this understanding to nonlinear response, specifically to the problem of second-harmonic generation in a reflection geometry.

Although such second-harmonic generation has been observed for over 20 years,^{7,8} its microscopic description has remained at a rather qualitative level—see the historical review in Ref. 9. Rudnick and Stern^{10,11} were the first to point out the need for a more careful analysis of the surface excitation mechanisms. They parametrized such effects in terms of two frequency-dependent numbers, a and b , which they estimated to be of order unity. In 1980 Sipe *et al.*¹² formulated a hydrodynamic theory of the generation process. Although they did not solve their equations in detail, they did confirm the estimates of Rudnick and Stern of the a and b parameters. In particular they showed that $b = -1$ well below the bulk plasma frequency ω_B , and suggested that there might be resonance structure in a near ω_B .

We have generalized their basic equations in order to account for ohmic damping and here present a numerical solution for the second-harmonic generation efficiency over a wide range of incident frequencies and angles. A brief derivation is given in Sec. II, which establishes our notation and motivates the additional boundary conditions (ABC's) necessary to calculate a solution. We also show how the a and b parameters may be defined and extracted from our model. Then in Sec. III we present our numerical results, changing various parameters in order to illustrate their qualitative influence. The results do confirm the theoretical suggestions of Sipe *et al.*¹²

No comparison with experiment is attempted because our model is probably too crude and arbitrary for such an

effort to be meaningful. The model treats only the nonlinear response of free electrons at a smooth surface and further approximates this by hydrodynamic equations. In its favor it should be noted that the model has been successful in linear response problems,^{3,13-16} yielding the same qualitative results as more sophisticated treatments but requiring much less computation. For the nonlinear response, its use here allows the first detailed microscopic treatment of the surface influence on both the induced polarization and the resulting radiation.

II. DERIVATION

The hydrodynamic model is based on a postulated equation of motion for the velocity field $\mathbf{v}(\mathbf{r}, t)$ of free electrons. We use here

$$\frac{\partial \mathbf{v}}{\partial t} + (\mathbf{v} \cdot \nabla) \mathbf{v} = \frac{e}{m} \left[\mathbf{E} + \frac{1}{c} \mathbf{v} \times \mathbf{B} \right] - \frac{1}{mn} \nabla p - \frac{1}{\tau} \mathbf{v}, \quad (1)$$

where \mathbf{E} and \mathbf{B} are electric and magnetic fields, respectively, and p is the pressure, which is assumed to depend only on the electron density n . The charge and mass of each electron are $e < 0$ and m , and c is the speed of light. Equation (1) differs from that used by Sipe *et al.*¹² by having a term for ohmic damping, parametrized by the constant scattering rate $1/\tau$. As they do, we assume that the relation between pressure and density is of the form

$$p(\mathbf{r}, t) = \zeta [n(\mathbf{r}, t)]^{5/3}, \quad (2)$$

with ζ constant. The value of ζ is discussed in Sec. III, but, like that of $1/\tau$, is irrelevant here.

To determine nonlinear effects, all the variables in (1) are expanded in a series of orders:

$$A = A_0 + A_1 + A_2 + \cdots, \quad (3)$$

with $A = \mathbf{v}$, \mathbf{E} , \mathbf{B} , or n , and a sequence of equations of fixed order are generated. Since the A_0 terms are equilibrium values, we assume that both \mathbf{v}_0 and \mathbf{B}_0 are zero. Then the expansion yields up through second order

$$0 = \frac{n_0 e}{m} \mathbf{E}_0 - \frac{5}{3m} \zeta n_0^{2/3} \nabla n_0, \quad (4a)$$

$$n_0 \left[\frac{\partial}{\partial t} + \frac{1}{\tau} \right] \mathbf{v}_1 = \frac{n_0 e}{m} \mathbf{E}_1 + \frac{n_1 e}{m} \mathbf{E}_0 - \frac{5}{3m} \zeta \nabla (n_0^{2/3} n_1), \quad (4b)$$

$$n_0 \left[\frac{\partial}{\partial t} + \frac{1}{\tau} \right] \mathbf{v}_2 + n_1 \left[\frac{\partial}{\partial t} + \frac{1}{\tau} \right] \mathbf{v}_1 + n_0 (\mathbf{v}_1 \cdot \nabla) \mathbf{v}_1 = \frac{n_0 e}{m} \mathbf{E}_2 + \frac{n_1 e}{m} \mathbf{E}_1 + \frac{n_2 e}{m} \mathbf{E}_0 \\ + \frac{n_0 e}{mc} \mathbf{v}_1 \times \mathbf{B}_1 - \frac{5}{3m} \zeta \nabla \left[n_0^{2/3} \left(n_2 + \frac{1}{3} \frac{n_1^2}{n_0} \right) \right]. \quad (4c)$$

Next, define a plasma frequency ω_0 and a velocity parameter β_0 by

$$\omega_0^2 = \frac{4\pi n_0 e^2}{m}, \quad (5)$$

$$\beta_0^2 = \frac{5}{3} \zeta n_0^{2/3} / m. \quad (6)$$

Further, introduce the electronic charge density $\rho = en$ and current density $\mathbf{j} = en\mathbf{v}$, which together satisfy order by order an equation of continuity. The formal solution of (4a) may then be written as

$$\mathbf{E}_0 = \frac{4\pi\beta_0^2}{\omega_0^2} \nabla \rho_0, \quad (7)$$

which we use to eliminate \mathbf{E}_0 from the higher-order equations. For instance, Eq. (4b) becomes

$$\left[\frac{\partial}{\partial t} + \frac{1}{\tau} \right] \mathbf{j}_1 = \frac{\omega_0^2}{4\pi} \mathbf{E}_1 - n_0 \nabla \left[\frac{\beta_0^2}{n_0} \rho_1 \right]. \quad (8)$$

Now imagine that one has externally manipulated \mathbf{E}_0 so that n_0 is a sequence of steps parallel to the surface. Within each step n_0 is constant and (8) becomes simply

$$\left[\frac{\partial}{\partial t} + \frac{1}{\tau} \right] \mathbf{j}_1 = \frac{\omega_0^2}{4\pi} \mathbf{E}_1 - \beta_0^2 \nabla \rho_1. \quad (9)$$

Across the interface between steps, where n_0 is discontinuous, we impose continuity of the normal component of \mathbf{j}_1 and of all the first-order electromagnetic fields. If we further wish that Eq. (8) remain nonsingular across the interface, these constraints require that $\beta_0^2 n_1 / n_0$ be continuous. These assumed continuity conditions provide the ABC's for the first-order quantities. As discussed elsewhere,¹⁷⁻²⁰ the choice of ABC's, like the form of Eq. (1), represents an ansatz. Our choice here is the usual one for electronic problems, but it is not the only possibility. Further, our simplification of the equilibrium density profile, while not absolutely necessary,^{21,22} greatly aids the solution of the model and avoids some of the intrinsic flaws of the hydrodynamic approach.^{19,23}

Turning now to the second-order Eq. (4c), we eliminate both \mathbf{E}_0 and \mathbf{E}_1 to find

$$\left[\frac{\partial}{\partial t} + \frac{1}{\tau} \right] \mathbf{v}_2 = \frac{e}{m} \left[\mathbf{E}_2 + \frac{1}{c} \mathbf{v}_1 \times \mathbf{B}_1 \right] + \mathbf{v}_1 \times (\nabla \times \mathbf{v}_1) \\ - \nabla \left[\frac{1}{2} (\mathbf{v}_1)^2 + \frac{\beta_0^2}{n_0} \left(n_2 - \frac{1}{6} \frac{n_1^2}{n_0} \right) \right]. \quad (10)$$

We again imagine that \mathbf{E}_0 has been chosen so n_0 is a sequence of steps and require that the other electromagnetic fields and the normal component of \mathbf{j}_2 be continuous across each interface. To extract a further ABC from (10), we use (8) to examine $\nabla \times \mathbf{v}_1$:

$$\left[\frac{\partial}{\partial t} + \frac{1}{\tau} \right] \nabla \times \mathbf{v}_1 = \nabla \times \left[\frac{\omega_0^2}{4\pi\rho_0} \mathbf{E}_1 - \nabla \left[\frac{\beta_0^2}{n_0} n_1 \right] \right] \\ = \frac{e}{m} \nabla \times \mathbf{E}_1 = - \frac{e}{mc} \frac{\partial \mathbf{B}_1}{\partial t}. \quad (11)$$

Thus, if we assume that \mathbf{v}_1 , \mathbf{v}_2 , \mathbf{E}_2 , and \mathbf{B}_1 are nonsingular through an interface, the whole Eq. (10) will be nonsingular if we impose continuity of

$$\frac{1}{2} (\mathbf{v}_1)^2 + \frac{\beta_0^2}{n_0} \left[n_2 - \frac{1}{6} \frac{n_1^2}{n_0} \right].$$

Hence we adopt this constraint, plus that on normal \mathbf{j}_2 , as our second-order ABC's.

We remark that the same ABC's can be obtained from an examination of Poynting's theorem.^{17,18} Setting $\mathbf{E}_0 = 0$, one finds that the energy current through third-order can be written as

$$\mathbf{G} = \frac{c}{4\pi} [\mathbf{E}_1 \times \mathbf{B}_1 + (\mathbf{E}_2 \times \mathbf{B}_1 + \mathbf{B}_2 \times \mathbf{E}_1)] \\ + \frac{4\pi\beta_0^2}{\omega_0^2} \left[\rho_1 \mathbf{j}_1 + \left[\rho_1 \mathbf{j}_2 + \rho_2 \mathbf{j}_1 - \frac{1}{6} \mathbf{j}_1 \frac{\rho_1^2}{\rho_0} \right. \right. \\ \left. \left. + \frac{1}{2\beta_0^2} \mathbf{j}_1 \frac{(\mathbf{j}_1)^2}{\rho_0} \right] \right]. \quad (12)$$

The continuity of the normal component of \mathbf{G} is possible if one imposes the boundary conditions outlined above. Thus, our choice of ABC's insures that each interface is neither a sink nor a source of energy as well as not a site of singular fields (except for \mathbf{E}_0) or charge accumulations.

Let us now summarize the particular hydrodynamic model developed here. We need the simultaneous solution of Maxwell's equations and the equation of motion of the electrons. Away from the interfaces of our stepped-density model, (7) is trivial, (8) is replaced by (9), and (10) may be rewritten as

$$\left[\frac{\partial}{\partial t} + \frac{1}{\tau} \right] \mathbf{j}_2 = \frac{\omega_0^2}{4\pi} \mathbf{E}_2 - \beta_0^2 \nabla \rho_2 + \mathbf{S}, \quad (13)$$

where

$$\begin{aligned} \mathbf{S} = & \frac{\omega_0^2}{4\pi\rho_0 c} (\mathbf{j}_1 \times \mathbf{B}_1) - \frac{1}{\rho_0} (\mathbf{j}_1 \cdot \nabla) \mathbf{j}_1 \\ & + \frac{\rho_1}{\rho_0} \left[\frac{\omega_0^2}{2\pi} \mathbf{E}_1 - \frac{5}{3} \beta_0^2 \nabla \rho_1 - \frac{1}{\tau} \mathbf{j}_1 \right]. \end{aligned} \quad (14)$$

The driving terms of the second-harmonic signal, Eq. (14), are consistent with those found by Sipe *et al.*,¹² if one notes that here n_0 is constant and $1/\tau$ nonzero. In addition to (9) and (13) in the homogeneous regions, we have across each interface the usual Fresnel boundary conditions and the ABC's. The problem to be solved has a plane electromagnetic wave of p -polarization incident from vacuum on the jellium, which lies in $x \geq 0$. All fields generated by this perturbation eventually travel away from the surface.

Our method of solution is that of partial waves,^{13,20} which has been amply described before for the first-order response.²⁴ After obtaining the first-order quantities, we find \mathbf{S} in (14) and then solve the inhomogeneous second-order Eq. (13). This last task we do by successively applying the boundary conditions. In bulk the partial-wave expansion has two unknowns: the coefficients of the decaying, homogeneous, transverse and longitudinal waves.¹³ In any other density step there are four unknowns since the partial waves can propagate there in either direction. At an internal interface we have four boundary-condition equations. Call the bulk the zeroth step. The boundary conditions at its interface with the first step determine the four first-step unknowns in terms of the two zeroth-step (bulk) unknowns. Then the boundary conditions between the first and second step determine the four second-step unknowns in terms of the first-step unknowns, hence in terms of the two bulk unknowns. This process is continued up to the last step and its interface with vacuum. There we can match on to only a single transverse wave, which alone can propagate into the vacuum. One has, at this point, three unknowns—the vacuum reflection amplitude and the two bulk unknowns. Hence, only one ABC is required, and we require the normal component of the current to vanish. This is consistent with (12) and avoids the ambiguity of expressions like n_1/n_0 or n_2/n_0 in vacuum where no density exists. Once the second-harmonic reflection amplitude is found, one can easily compute R defined as the ratio of the reflected second-harmonic Poynting flux to the square of the incident first-harmonic Poynting flux.

Before describing the numerical results, we compare our method of solution to that proposed by Sipe *et al.*¹² They modify the analogues of (9) and (13) to account for

the different spatial range of longitudinal and transverse waves before trying to solve these equations. We do not follow this procedure since it is of no particular advantage in a numerical solution. Instead, the polarization and reflected radiation are simultaneously computed. However, after this is done, we can extract the a and b parameters and examine their sense and structure. This is done as follows.

Begin by introducing the polarization \mathbf{P} , where $\mathbf{j} = \partial \mathbf{P} / \partial t$ and $\rho = -\nabla \cdot \mathbf{P}$. Further, replace all variables by their complex amplitudes. Since at each order frequency and surface wave vector are the same, we can write for instance the m th order polarization \mathbf{P}_m as

$$\mathbf{P}_m(\mathbf{x}, t) = 2 \operatorname{Re}[\mathbf{P}_m(x) e^{-im(\omega t - \underline{Q} \cdot \underline{X})}], \quad (15)$$

where $m = 1$ or 2 and Re denotes "real part of." The two-dimensional vectors \underline{Q} and \underline{X} lie in the surface plane while x runs along its normal. The incident radiation from vacuum is at frequency ω and $\underline{Q} = (\omega/c) \sin \theta$, where θ is the angle of incidence (and reflection). We use the same symbol for a physical variable [e.g., \mathbf{P}_m on the left side of (15)] and its complex amplitude [\mathbf{P}_m on the right-hand side of (15)], since the meaning is clear from the context. One can easily check that our previous equations also hold for the complex amplitudes, if one replaces $\partial/\partial t$ by $-im\omega$, etc.²⁵

With this new notation we can now describe the prescription for the a , b , and d parameters. One replaces (13) by

$$-\tilde{\Omega}^2 \mathbf{P}_2 = \left[\frac{\omega_B^2}{4\pi} \mathbf{E}_2 + \mathbf{S}_B \right] \Theta(x) + \mathbf{S}_S, \quad (16)$$

where $\tilde{\Omega}^2 = \Omega(\Omega + i/\tau)$ with $\Omega = 2\omega$, ω_B is the bulk plasma frequency, \mathbf{S}_S is another driving term to be specified later, and $\Theta(x) = 1$ for $x > 0$ and zero otherwise. The driving term \mathbf{S}_B is determined by an approximate version of the long-range piece of the first term in (14)

$$\mathbf{S}_B = -i \frac{\omega e}{mc} \mathbf{P}_1 \times \mathbf{B}_1, \quad (17)$$

where \mathbf{P}_1 and \mathbf{B}_1 are determined not from (9) and its ABC's, but instead from

$$-\tilde{\omega}^2 \mathbf{P}_1 = \left[\frac{\omega_B^2}{4\pi} \mathbf{E}_1 \right] \Theta(x), \quad (18)$$

where $\tilde{\omega}^2 = \omega(\omega + i/\tau)$ and, as in (16), one has neglected spatial dispersion and used the bulk electron density up to the vacuum interface at $x = 0$. The Fresnel boundary conditions suffice to determine these first-order fields. For our geometry one quickly finds

$$\mathbf{S}_B = -\tilde{\Omega}^2 \gamma d \nabla (\mathbf{E}_1)^2, \quad (19)$$

where

$$\gamma = -\frac{e}{8\pi m} \frac{\omega_B^2}{\tilde{\omega}^2 \tilde{\Omega}^2} \quad (20)$$

and

$$d = 1. \quad (21)$$

The γ of (20) is the analogue of the same quantity introduced by Sipe and Stegeman.⁹ It becomes identical to theirs when $1/\tau=0$. We have chosen the definition (20) so that d is one at all frequencies. Deviations from this value can arise only if one goes beyond a jellium description of the bulk metal.

The other driving term in (16) is a δ function located just outside the metal surface

$$\mathbf{S}_S = -\tilde{\Omega}^2 \mathbf{D} \delta(x + 0^+), \quad (22)$$

where

$$\mathbf{D} = \int_0^{d_L} dx \mathbf{P}_2^{(s)}. \quad (23)$$

Here $\mathbf{P}_2^{(s)}$ is the part of the exact polarization that is driven by terms that vary rapidly and d_L is a distance large enough for these fields to have vanished, but small enough that \mathbf{S}_B has negligibly changed. The existence of d_L depends on the large difference between any β_0 and c , which determine the normal component of homogeneous, longitudinal and transverse waves, respectively. For longitudinal waves in bulk these wave-vector components are¹³

$$p_L = \left[\frac{\tilde{\omega}^2 - \omega_B^2}{\beta_B^2} - Q^2 \right]^{1/2} \quad (24)$$

for the first harmonic and

$$p_L = \left[\frac{\tilde{\Omega}^2 - \omega_B^2}{\beta_B^2} - K^2 \right]^{1/2} \quad (25)$$

for the second harmonic, with $K=2Q$. The analogous transverse quantities are¹³

$$p_T = \left[\frac{\omega^2}{c^2} \left[1 - \frac{\omega_B^2}{\tilde{\omega}^2} \right] - Q^2 \right]^{1/2}, \quad (26)$$

$$p_T = \left[\frac{\Omega^2}{c^2} \left[1 - \frac{\omega_B^2}{\tilde{\Omega}^2} \right] - K^2 \right]^{1/2}. \quad (27)$$

Since in metals β_B is approximately the Fermi velocity, which in turn is roughly 2 orders of magnitude smaller than the speed of light, the definition of $\mathbf{P}_2^{(s)}$ and d_L are reasonably meaningful if not precise.

The a and b parameters serve to parametrize the \mathbf{D} due to an incident p -polarized wave. We write

$$\hat{\mathbf{x}} \cdot \mathbf{D} = -\frac{a}{2} [\hat{\mathbf{x}} \cdot \mathbf{E}_1(0^+)]^2 \left[\gamma \frac{\tilde{\Omega}^2}{\tilde{\omega}^2} \right], \quad (28)$$

$$\hat{\mathbf{Q}} \cdot \mathbf{D} = -b [\hat{\mathbf{x}} \cdot \mathbf{E}_1(0^+)] [\hat{\mathbf{Q}} \cdot \mathbf{E}_1(0^+)] \left[\gamma \frac{\tilde{\Omega}^2}{\tilde{\omega}^2} \right]. \quad (29)$$

The component of \mathbf{D} normal to the plane of incidence is zero. Our definitions reduce to those used before⁹⁻¹² when $1/\tau=0$. The \mathbf{E}_1 used here is to be calculated from (18) and we need the components just inside the metal.

Given a , b , and d , the sources in (16) are completely specified and one can calculate the resulting radiation. Before writing out the final result we summarize the approximations that lie behind it. In Eq. (16) for \mathbf{P}_2 one ignores density variations near the surface and nonlocal

response. Inside the metal only the extended source polarization, which varies as $e^{2ip_T x}$, is kept and its amplitude is approximated by a single-step Fresnel theory. The polarization produced by the other contributions to \mathbf{S} in (14) is first properly calculated via (13), then lumped into an effective δ function source term placed outside the metal. The radiation due to both of these effective sources is calculated from local optics to yield a second-harmonic generation efficiency of

$$R = \frac{8\pi e^2}{m^2 \omega^2 c^3} |r|^2, \quad (30)$$

where

$$r = \frac{\omega^2}{\tilde{\omega}^2} (\epsilon - 1) \alpha_0^2 \frac{Q\epsilon/2}{P_v \mathcal{E} + P_T} \left[a \left(\frac{Qc}{\omega} \right)^2 \frac{\mathcal{E}}{\epsilon} - b \frac{p_T p_T c^2}{\omega^2 \epsilon} + 2d \frac{\tilde{\omega}^2}{\tilde{\Omega}^2} \right]. \quad (31)$$

Here $\epsilon = 1 - \omega_B^2/\tilde{\omega}^2$, $\mathcal{E} = 1 - \omega_B^2/\tilde{\Omega}^2$, and α_0 is the Fresnel transmission amplitude

$$\alpha_0 = \frac{2p_v}{p_v \epsilon + p_T}. \quad (32)$$

The p_v and P_v in these equations are the normal components of transverse waves in vacuum: $\omega \cos \theta / c$ and $\Omega \cos \theta / c$, respectively. We show in the next section that the a , b , and d parameters are in the hydrodynamical model nearly independent of Q and (except for a) of ω . We also illustrate how well the parametrization scheme of (30) and (31) for R works.

III. RESULTS AND DISCUSSION

To extract numerical results from our model we must specify the various parameters it contains: ζ , $1/\tau$, and $n_0(x)$. We use the values that are successful in fitting the linear surface response of Al.³ The bulk density is determined by an r_s of 2.07, so $\hbar \omega_B = 15.8$ eV. The value of ζ in (2) is chosen so that $\beta_0^2 = \frac{3}{5} v_{F,0}^2$, where $v_{F,0}$ is the (local) Fermi velocity. We solve the model for two different surface profiles. In the first the equilibrium density drops from its bulk value to zero in one step, while in the second an intermediate step is added. This additional step has a width w of a few angstroms and is assigned a density equal to 0.7 of the bulk density. When $w = 4$ Å, the surface plasmon dispersion predicted by the hydrodynamic model is in good agreement with experiment.²⁶ For $w \geq 1.7$ Å the hydrodynamic model further predicts the existence of an extra collective surface mode,¹⁶ often called a multipole surface plasmon.^{27,28} A second such mode appears above $w = 5.1$ Å. For completeness we have done calculations for $0 \leq w \leq 6$ Å. The value of $1/\tau$ is such that $\omega_B \tau = 10$ everywhere. This rather large scattering rate is often necessary in hydrodynamic calculations because one is trying to restore the Landau damping omitted by the model. However, since the latter depends significantly on frequency, wave vector, and density, while our $1/\tau$ is independent of all of these, one has only a crude representation of the damping.

In Fig. 1 we show the second-harmonic generation efficiency R for the one-step model. For $\omega \ll \omega_B$, R increases quadratically with ω with a strength that depends on θ . This growth saturates as ω approaches $\omega_B/2$ and then R drops quickly with further increases in ω . The largest values of R occur away from either extreme in θ : at large θ (or small ω) the linear signal does not penetrate the metal, while at small θ the induced value of n_1 is negligible. There are minor refinements in this description that are easily seen in Fig. 1. At large θ a ridge in R extends up through ω_B , and at small θ a plateau beyond the main peak is centered on ω_B . For intermediate θ there is a shallow depression along $\omega = \omega_B/2$. The loci of the ridge and the upper edge of the plateau follow, respectively, the curves $\Omega \cos \theta = \omega_B$ and $\omega \cos \theta = \omega_B$, which in turn describe roughly when the transverse waves change from decaying to propagating into the bulk. The structure along $\omega = \omega_B/2$ is similarly related to when longitudinal waves at the second harmonic can propagate into the bulk, although R shows no analogous effect at the first harmonic, i.e., along $\omega = \omega_B$.

We next consider the parametrization scheme (30) and (31) with a , b , and d . For our model $d = +1$ everywhere and we show in Fig. 2 the frequency dependence of a and b (Ref. 29) as well as both the exact R and its approximation via (30) and (31). We have arbitrarily set $\theta = 60^\circ$ in drawing this figure since we find that the variation of a and b with θ at fixed ω is less than a few percent over the whole range of θ except for $\theta \ll 1^\circ$. Similarly, although R varies with θ as shown in Fig. 1, the agreement between the exact and approximate R is as good as shown in Fig. 2 for any θ , except as $\theta \rightarrow 0$ where both are negligible. Thus, all the information in Fig. 1 is implicit in Fig. 2 and Eqs. (30) and (31).

The reason for this general success of (30) and (31) lies in the small value of β_B compared to c and in the large damping $1/\tau$. If we further decrease β_B the agreement becomes better, while increasing β_B by a factor of 10 leads to variations in a and b with θ and a mismatch between the exact R and that of (30) and (31) all of about 20%.

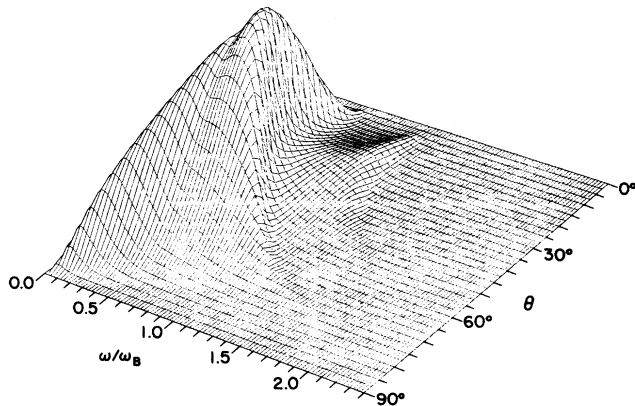


FIG. 1. Second-harmonic generation efficiency R versus frequency and angle of incidence for a single-step equilibrium density profile. We plot R on a linear scale, and its maximum value is $1.4 \times 10^{-20} \text{ cm}^2/\text{W}$, which occurs at $\theta = 45^\circ$ and $\omega/\omega_B = 0.60$.

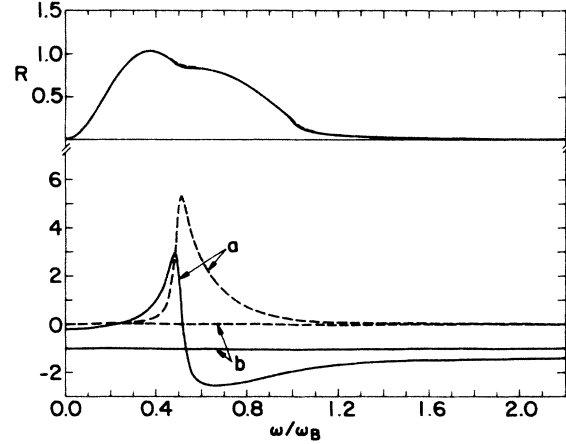


FIG. 2. Frequency dependence of second-harmonic generation parameters. In the lower panel the real parts of a and b are drawn with solid lines, the imaginary parts with dashed lines. The imaginary part of b is essentially zero. The upper panel compares the exact R , the solid line, and that calculated from (30) and (31), the dashed line. Both are in units of $10^{-20} \text{ cm}^2/\text{W}$.

Indeed it is the small size of β_B/c that underlies the considerable progress in the analysis of linear properties (Refs. 2, 4–6, 30, and 31), so one should expect to (and does) see it simplifying the second-harmonic results.¹² Still the prescription for extracting a and b described in Sec. II does not seem reasonable above $\omega_B/2$, since then some of the contributions which are formally lumped into a surface δ function in fact can propagate into the bulk. However, the period of these oscillations is generally of the order of angstroms, and even when this fails (near $\omega_B/2$ and ω_B) one still has the damping to help localize these driving terms.

Now consider the numerical values of the a and b parameters, noting first that b is essentially the constant -1 . This value is held to within a few percent for all ω and (almost) all θ . It is only in the frequency dependence of a that a significant variation occurs. As shown in Fig. 2, a has a sharp structure near $\omega_B/2$. This becomes even sharper when $1/\tau$ is decreased. We have determined that this structure in a is due to a factor of P_L^{-1} , which diverges at $\omega = \omega_B/2$ when $1/\tau = 0$. No such singularity occurs at ω_B . Further, the sharp peak in a at $\omega_B/2$ does not produce a corresponding peak in R due to the compensating factor of \mathcal{E} multiplying a in (31). It is this factor of \mathcal{E} that is directly responsible for the local minimum in R at $\omega_B/2$ in Fig. 1.

Next we examine a model with two steps in the equilibrium density profile. In Fig. 3 we show how R at a fixed angle of incidence develops structure in its frequency dependence as the width of the intermediate density step between vacuum and bulk is increased. At a qualitative level, the structure is due to standing waves in the overlayer; but, since several wave vectors are involved and because all of the partial waves can leak out of the overlayer to some extent, the ridges in Fig. 3 that move downward in ω as w increases do not follow simple loci. This is

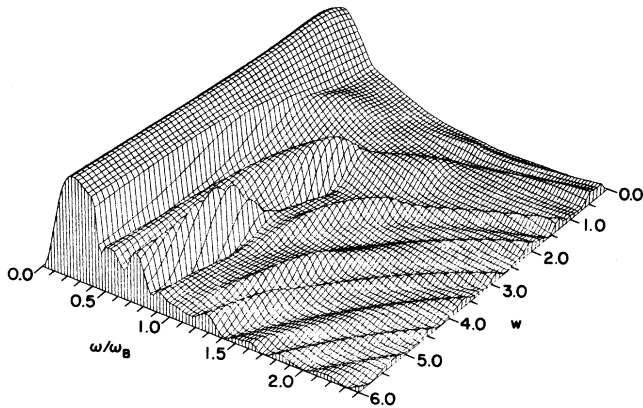


FIG. 3. Second-harmonic generation efficiency R versus frequency and step width for a two-step equilibrium density profile. The angle of incidence is 70° . We plot R on a linear scale, and its maximum value is $0.8 \times 10^{-20} \text{ cm}^2/\text{W}$, which occurs at $w=0.7 \text{ \AA}$ and $\omega/\omega_B=0.25$.

especially evident when a ridge drops below ω_B . Above ω_B the ridges roughly follow either $p_L w = \text{constant}$ or $P_L w = \text{constant}$ with $1/\tau$ ignored and the overlayer density used in the wave vector, but the ones that go below ω_B seem to change direction. One might guess that the ridges are then following the multipole locations. However, a comparison with Fig. 4, which plots the multipole frequencies for the two-step model, shows that this ansatz is untenable. The strong structure in R is not simply related to first-order response properties.

In Fig. 5 we plot R as in Fig. 1, but now with $w=4 \text{ \AA}$. The various ridges in Fig. 3 here appear at fixed ω over a range of angles. Below ω_B the structure extends over nearly the whole range of θ , while above ω_B the mounds disappear for $\theta < \cos^{-1}(\omega_B/\omega)$ and peak near $\theta = \cos^{-1}(\omega_B/\Omega)$. The physical interpretation of these

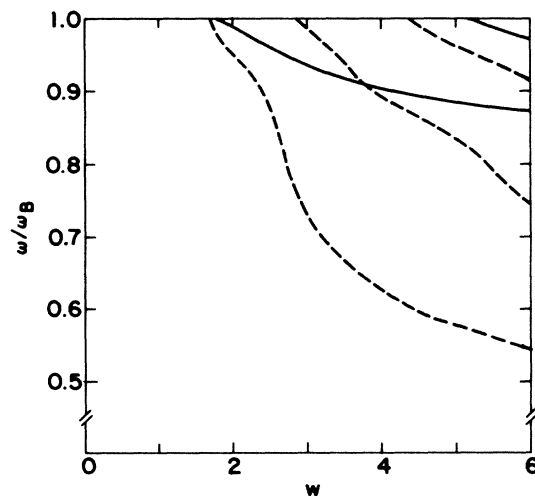


FIG. 4. Locations in frequency of multipole modes (—) and maxima in second-harmonic generation efficiency (---) versus overlayer width w in angstroms. An angle of incidence of 70° is used for the calculation of R . The multipole modes are found from the nonretarded, zero parallel wave-vector limit described in Ref. 16.

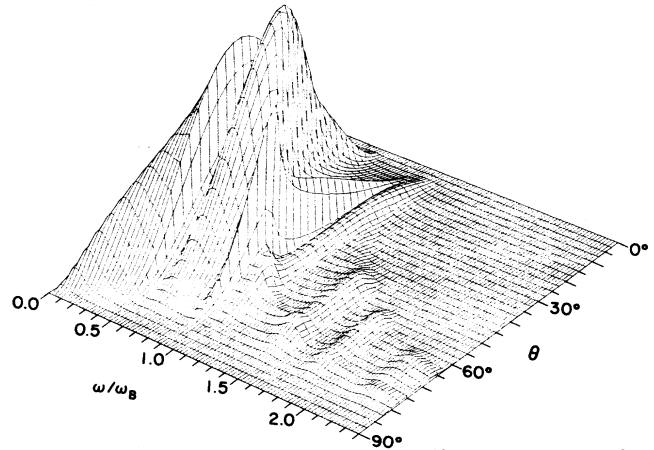


FIG. 5. Second-harmonic generation efficiency R versus frequency and angle of incidence for a two-step equilibrium density profile with $w=4 \text{ \AA}$. We plot R on a linear scale and its maximum value is $1.8 \times 10^{-20} \text{ cm}^2/\text{W}$, which occurs at $\theta=45^\circ$ and $\omega/\omega_B=0.625$.

limits was noted earlier. Compared to Fig. 1, the magnitude of R is roughly the same, but it now exhibits much more structure as a function of frequency. At fixed frequency below ω_B , R has qualitatively the same θ dependence as in the absence of the overlayer. Hence, it would be more fruitful in experiments to sweep ω at fixed θ , rather than vice versa.

The parametrization scheme for R based on (30) and (31) continues to work nearly as well as when $w=0$. This is illustrated in Fig. 6 for the case $w=4 \text{ \AA}$. As in Fig. 2 we only show results at $\theta=60^\circ$, since neither a , b , nor the

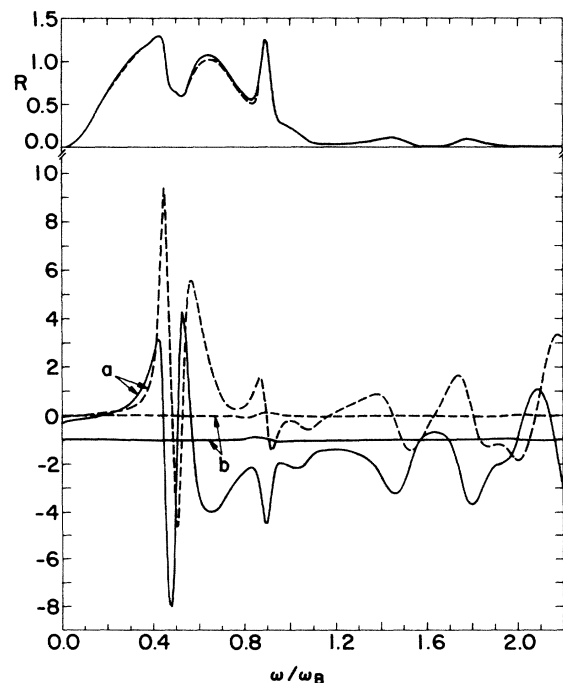


FIG. 6. Frequency dependence of second-harmonic generation parameters. The plotting scheme is the same as in Fig. 2, but here the width of the intermediate step is 4 \AA .

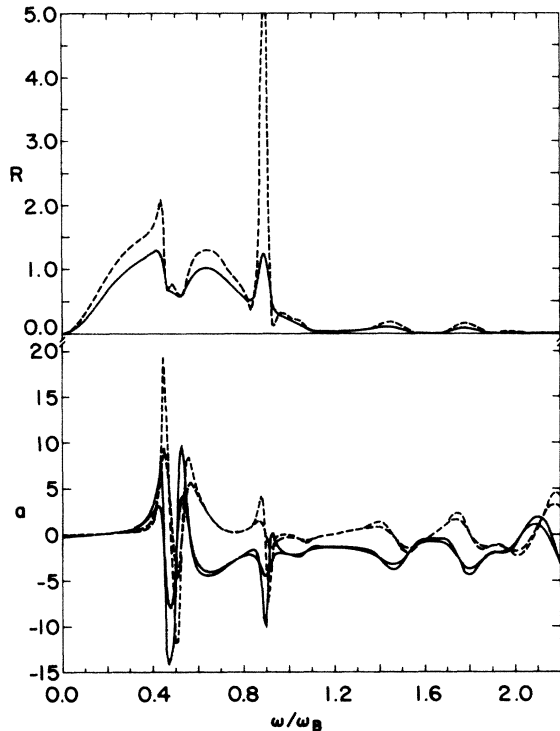


FIG. 7. Dependence of R and a on the strength of ohmic damping. We use either $\omega_B\tau=10$ or $\omega_B\tau=20$, with the latter yielding stronger structure. In the upper panel, the units of R are 10^{-20} cm²/W and the off-scale peak rises to 6.8. In the lower panel the real part of a is denoted by a solid line, and the imaginary part by a dashed line. We have not shown b since in both cases it is essentially -1 .

ratio between the R 's has a significant dependence on θ . The additional peaks in R , compared to Fig. 2, are due to extra structure in a ; b remains essentially -1 . The amplitude of the oscillations in a is growing for $\omega > \omega_B$, but that of $\hat{\mathbf{x}} \cdot \mathbf{D}$ in (28) is not. Furthermore, once the frequency surpasses $\omega_B/\cos\theta$ the structure in a is no longer evident in R . As noted earlier, the new structures arise from standing waves in the intermediate step although their

precise location is not amenable to a simple expression. We did check that increasing both β_0 and w by the same factor leads to essentially no shift in frequency of the peak positions in Fig. 6.

Finally we comment on the strength and sharpness of the structure we have found in R and a . These features can depend quite sensitively on the value of $1/\tau$ used in the model. This is illustrated in Fig. 7, where we compare the R and a values for two different choices of $1/\tau$. In general a decrease in $1/\tau$ leads to a sharpening of the structure, but the influence of $1/\tau$ is not the same for all peaks. Those above ω_B are all only slightly affected, while those below ω_B are extremely sensitive only if they lie close in frequency to a multipole mode. Still there is enough dependence on $1/\tau$ to remind one that the hydrodynamic model can only make qualitative predictions.

To summarize, our calculations suggest that considerable structure exists in the frequency dependence of second-harmonic generation at a metal surface. On the experimental side, it would be interesting to have data taken on a free-electron-like material in the vicinity of ω_B in order to confirm our predictions and to refine our choice of parameters. Since the parametrization scheme with a , b , and d appears to work quite well, the key measurement is the frequency dependence of a . On the theoretical side, there is also a need for considerable further work. At the level of a jellium model, one must learn how to include consistently the effect of both the Landau damping and the continuous, smooth, surface density profile. One needs further to go beyond the jellium model, to develop tractable estimates of the influence of core polarization and band structure. These tasks are easily stated, but their accomplishment will require considerable work. We hope that they will be attempted soon.

ACKNOWLEDGMENTS

This work was supported in part by the National Science Foundation through Grant No. DMR-81-15705. One of us (M.C.) gratefully acknowledges support from the Galileo Galilei Foundation.

¹G. Mukhopadhyay and S. Lundqvist, *Phys. Scr.* **17**, 69 (1978).
²P. Apell, *Phys. Scr.* **24**, 795 (1981).
³F. Forstmann and R. R. Gerhardt, *Festkörperprobleme: Advances in Solid State Physics*, edited by J. Treush (Vieweg, Braunschweig, 1982), Vol. XXII, p. 291.
⁴P. J. Feibelman, *Prog. Surf. Sci.* **12**, 287 (1982).
⁵P. Apell, A. Ljungbert, and S. Lundqvist, *Phys. Scr.* **30**, 367 (1984).
⁶F. Flores and F. Garcia-Moliner, in *Surface Excitations*, edited by V. M. Agranovich and P. Loudon (North-Holland, New York, 1984).
⁷N. Bloembergen, *Nonlinear Optics* (Benjamin, New York, 1965).
⁸Y. R. Shen, *The Principles of Nonlinear Optics* (Wiley, New York, 1984).

⁹J. E. Sipe and G. I. Stegeman, in *Surface Polaritons*, edited by V. M. Agranovich and D. L. Mills (North-Holland, New York, 1982).
¹⁰J. Rudnick and E. A. Stern, *Phys. Rev. B* **4**, 4274 (1971).
¹¹J. Rudnick and E. A. Stern, *Polaritons*, edited by E. Burstein and F. DeMartini (Plenum, New York, 1974).
¹²J. E. Sipe, V. C. Y. So, M. Fukui, and G. I. Stegeman, *Solid State Commun.* **34**, 523 (1980); *Phys. Rev. B* **21**, 4389 (1980).
¹³C. Schwartz and W. L. Schaich, *J. Phys. C* **17**, 537 (1984).
¹⁴K. Kempa and F. Forstmann, *Surf. Sci.* **129**, 516 (1983).
¹⁵G. Piazza, D. M. Kolb, K. Kempa, and F. Forstmann, *Solid State Commun.* **51**, 905 (1984).
¹⁶C. Schwartz and W. L. Schaich, *Phys. Rev. B* **30**, 1059 (1984).
¹⁷F. Forstmann, *Z. Phys. B* **32**, 385 (1979).
¹⁸W. L. Schaich and C. Schwartz, *Phys. Rev. B* **25**, 7365 (1982).

- ¹⁹C. Schwartz and W. L. Schaich, Phys. Rev. B **26**, 7008 (1982).
- ²⁰A. D. Boardman, in *Electromagnetic Surface Modes*, edited by A. D. Boardman (Wiley, New York, 1982).
- ²¹A. J. Bennett, Phys. Rev. B **1**, 203 (1970).
- ²²N. D. Lang, in *Solid State Physics*, edited by H. Ehrenreich, F. Seitz, and D. Turnbull (Academic, New York, 1973), Vol. 28.
- ²³P. Ahlqvist and P. Apell, Phys. Scr. **25**, 587 (1982).
- ²⁴References 13 and 20 describe the general method, but in fact use different ABC than those we presently employ.
- ²⁵The 2 in (15) is necessary for this check in (13).
- ²⁶F. Forstmann and H. Stenschke, Phys. Rev. B **17**, 1489 (1978).
- ²⁷A. Eguluz, S. C. Ying, and J. J. Quinn, Phys. Rev. B **11**, 2118 (1975).
- ²⁸A. Eguluz and J. J. Quinn, Phys. Rev. B **14**, 1347 (1976).
- ²⁹For the partial wave in the bulk that varies as $e^{iP_T x}$ we use $d_L = w + 2 \text{ \AA}$ in (23), while for all other partial waves we set $d_L = \infty$.
- ³⁰J. E. Sipe, Surf. Sci. **84**, 75 (1979).
- ³¹J. E. Sipe, Phys. Rev. B **22**, 1589 (1980).